

# HyperDet: 3D Object Detection with Hyper 4D Radar Point Clouds

Yichun Xiao<sup>1</sup>, Runwei Guan<sup>2</sup>, Fangqiang Ding<sup>3,†</sup>

**Abstract**—4D mmWave radar provides weather-robust, velocity-aware measurements and is more cost-effective than LiDAR. However, radar-only 3D detection still trails LiDAR-based systems because radar point clouds are sparse, irregular, and often corrupted by multipath noise, yielding weak and unstable geometry. We present **HyperDet**, a detector-agnostic radar-only 3D detection framework that constructs a task-aware *hyper* 4D radar point cloud for standard LiDAR-oriented detectors. **HyperDet** aggregates returns from multiple surround-view 4D radars over consecutive frames to improve coverage and density, then applies geometry-aware cross-sensor consensus validation with a lightweight self-consistency check outside overlap regions to suppress inconsistent returns. It further integrates a foreground-focused diffusion module with training-time mixed radar-LiDAR supervision to densify object structures while lifting radar attributes (e.g., Doppler, RCS); the model is distilled into a consistency model for single-step inference. On MAN TruckScenes, **HyperDet** consistently improves over raw radar inputs with VoxelNeXt and CenterPoint, partially narrowing the radar-LiDAR gap. These results show that input-level refinement enables radar to better leverage LiDAR-oriented detectors without architectural modifications.

## I. INTRODUCTION

3D object detection is a core component of spatial perception for mobile autonomous systems. It estimates the 3D state of surrounding objects, including position, size, orientation, and semantic attributes, enabling downstream modules such as tracking, motion prediction, and planning. Most approaches rely on cameras, LiDAR, or their fusion [1]. However, these sensors can degrade significantly in adverse weather (e.g., rain, snow, and fog) due to reduced visibility and corrupted signals, leading to missed detections and inaccurate boxes [2], posing risks to safety-critical applications.

Due to its sensing characteristics, mmWave radar is hardly affected by adverse weather and provide partial velocity measurement and is much cheaper than LiDARs. However, conventional automotive radars have limited azimuth resolution and weak elevation observability, resulting in sparse and ambiguous geometry that is inadequate for fine-grained 3D perception. Consequently, radar-only 3D detection still falls far behind LiDAR-based systems on established benchmarks [3], [4]. Recent advances in hardware and signal processing, especially MIMO antenna arrays, have improved angular resolution without requiring dense arrays, giving rise to modern 4D radars that extend range–azimuth–Doppler

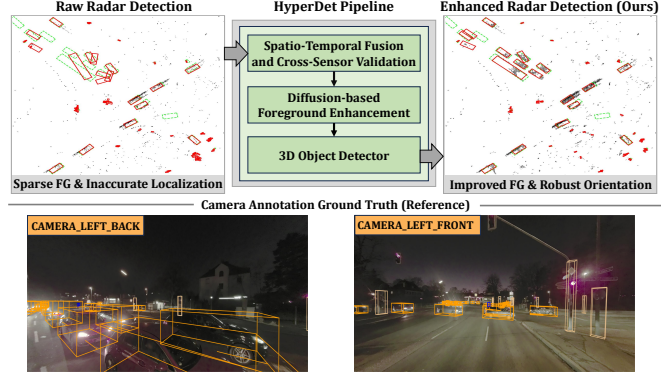


Fig. 1. **HyperDet** enhances 4D radar input quality and improves 3D localization and orientation over raw radar. Camera annotations are for reference. Red boxes denote predictions; green boxes denote ground truth.

with elevation-aware measurements [5]. These developments motivate renewed interest in whether 4D radar can narrow the radar-LiDAR performance gap for 3D perception.

Recent studies have explored 4D radar for 3D object detection [6]. Many methods follow LiDAR-oriented detection pipelines and take raw radar point clouds as network inputs, with gains largely attributed to architectural tweaks for feature extraction [7]–[9]. In practice, performance is frequently limited by the input itself: radar point clouds are very sparse and irregular, and they are often corrupted by multipath noises [10] (see Fig. 1). As a result, downstream detectors operate on weak and unstable geometric cues, leading to unreliable predictions in complex traffic scenes. This suggests that the key bottleneck lies in *input quality* rather than detector design, motivating a detector-agnostic radar front-end that constructs a denser and cleaner radar representation before applying standard 3D detectors.

To tackle these challenges, we present **HyperDet**, a radar-only 3D detection pipeline that improves radar perception at the input level by building a task-aware *hyper* 4D radar point cloud to mitigate the inherent sparsity and noise of radar measurements. To mitigate the sparsity, **HyperDet** aggregates radar returns from multiple surround-view 4D radar sensors over consecutive frames, improving spatial coverage and point density. However, such spatio-temporal fusion can also accumulate and amplify sensor-specific noise across views and sweeps. To curb this effect, we exploit the multi-radar setup and introduce a geometry-aware cross-sensor consensus validation mechanism: within overlapping fields of view, we remove reflections that are inconsistent across radars, and further complement it with a lightweight self-consistency check to avoid over-filtering sparse yet valid returns outside overlap regions.

Despite cross-sensor validation, radar-only detection re-

<sup>†</sup>Corresponding author

<sup>1</sup>Yichun Xiao is with School of Informatics, University of Edinburgh, Edinburgh, United Kingdom

<sup>2</sup>Runwei Guan is with Thrust of Artificial Intelligence, Hong Kong University of Science and Technology (Guangzhou), Guangzhou, China.

<sup>3</sup>Fangqiang Ding is with Department of Mechanical Engineering, Massachusetts Institute of Technology, Boston, USA. fding@mit.edu

mainly input-limited: the fused point cloud is still sparse and irregular, and a portion of noisy returns cannot be reliably validated outside overlap regions, leading to weak and unstable foreground geometry. To further enhance the detector input, HyperDet integrates a diffusion-based *foreground* enhancement module motivated by the denoising and reconstruction capabilities of diffusion models [11]. Rather than reconstructing a globally dense scene [12], which can be dominated by background and include structures irrelevant to detection, we target object-level foreground geometry that directly supports 3D bounding box regression. LiDAR is used only during training to provide explicit supervision. Specifically, we guide the diffusion process with a fused radar–LiDAR object representation that preserves the radar background while injecting LiDAR-derived structure within object regions. This enables the model to densify and regularize foreground shapes without shifting to full-scene reconstruction. To preserve radar-specific characteristics, we associate the enhanced foreground with radar attributes (e.g., Doppler and RCS) via a simple attribute lifting scheme from nearby raw returns. For real-time inference speed, we distil the diffusion model into a consistency model [13] to enable efficient single-step sampling.

Building on the above, HyperDet forms a hierarchical input refinement pipeline comprising spatio-temporal multi-radar aggregation, cross-sensor consensus validation, and diffusion-based foreground enhancement, producing a task-aware *hyper* point cloud tailored for radar-only 3D detection (see Fig. 1). Evaluated on MAN TruckScenes [14] with both voxel- and point-based 3D detectors, i.e., VoxelNeXt [15] and CenterPoint [16], HyperDet achieves consistent improvements over raw radar inputs, partially narrowing the radar–LiDAR performance gap. We further evaluate diffusion-based enhancement with geometric fidelity metrics, conduct component-wise ablations, and report qualitative results and end-to-end efficiency with a consistency-distilled student for practical inference.

Our contributions are summarized as follows:

- We propose HyperDet, a radar-only 3D detection pipeline that constructs a task-aware *hyper* 4D radar point cloud as input to LiDAR-oriented detectors..
- We introduce spatio-temporal radar data aggregation to increase point density, together with a geometry-aware cross-sensor validation scheme that suppresses noisy points and inconsistent returns during fusion.
- We design a foreground-prioritized diffusion enhancement module with training-time mixed radar–LiDAR supervision to recover dense and coherent object-level structures critical for 3D detection, while preserving radar-specific characteristics (e.g., Doppler and RCS).
- Extensive experiments on public dataset with standard LiDAR detectors demonstrate consistent gains over radar-only baselines and a reduced radar–LiDAR performance gap. We will release our code and models.

## II. RELATED WORKS

### A. LiDAR-based 3D Object Detection

LiDAR is a primary sensing modality in autonomous driving, providing accurate 3D geometry as point clouds. Since these point sets are sparse and unordered, LiDAR-based detectors typically adopt a *representation–backbone–head* design to enable effective learning and inference [17]. Common representations include grid-based voxel/pillar encodings, point/graph formulations operating on raw points, and projection-based views such as bird’s-eye view (BEV), balancing geometric fidelity and context aggregation against computational efficiency [18]–[20]. Representative detectors span voxel-based pipelines (e.g., VoxelNet [21], SECOND [22]), efficient pillar-based designs (e.g., PointPillars [23]), and center-based BEV detectors (e.g., CenterPoint [16]); comprehensive surveys summarize their evolution and benchmark performance [19], [24].

### B. Radar-based 3D Object Detection

Radar-based 3D perception has evolved from conventional automotive radars that measure range–azimuth–Doppler to modern 4D mmWave radars that additionally observe elevation, improving angular resolution and providing denser measurements [4], [25], [26]. Early radar-only detection methods often followed LiDAR/camera-style pipelines by casting radar measurements into compatible representations and reusing mature detection architectures, with limited radar-specific designs [27]. With the increasing availability of 4D radars, recent radar-only detection research has progressed along two complementary directions. The first line improves input quality and consistency via temporal modelling and filtering, such as multi-frame accumulation [28], motion compensation [29], and adaptive filtering [30]. The second line extends LiDAR-style voxel/pillar/BEV detectors to radar and introduces architecture-level modifications for improved feature extraction [7]–[9], with representative examples including RadarPillars [8] and RadarGNN [31]. Despite steady progress, many methods still feed raw radar point clouds into detectors, leaving performance constrained by inherent sparsity and noise. In contrast, our work focuses on refining radar inputs so that standard LiDAR detectors can be exploited more effectively in the radar-only setting.

### C. Radar Point Cloud Enhancement

Radar point cloud enhancement methods can be broadly categorized into pre-/post-processing and cross-modal learning. Pre-processing includes adaptive CFAR variants [32] and learning-based clutter suppression and angular resolution enhancement [33], but these steps may remove valid detections and still yield sparse outputs. Post-processing leverages neural networks (e.g., PointNet [34], [35], cGANs [36], [37], and U-Nets [38], [39]) for denoising and super-resolution, while cross-modal frameworks exploit LiDAR supervision to generate pseudo-LiDAR structures or refine radar representations/heatmaps [40]–[42]. Diffusion models

have recently been explored for stochastic radar super-resolution and artifact suppression, either producing LiDAR-like dense point clouds [43] or reconstructing high-resolution radar representations with LiDAR-guided learning and fast inference [12]. Beyond enhancement, diffusion has also been applied to other 4D radar tasks (e.g., scene flow and motion segmentation) to handle noisy measurements [44]. Different from prior work that targets global super-resolution or modality translation, our approach is *detection-driven*: we first construct a task-aware hyper point cloud via spatio-temporal multi-radar fusion with cross-sensor validation, and then perform foreground-prioritized diffusion enhancement to recover object-level structures most critical for downstream 3D detection while preserving radar-specific attributes.

### III. METHODOLOGY

#### A. Task Definition

In this work, we introduce HyperDet, a 4D radar-only perception pipeline that refines multi-radar observations within a short temporal window to construct an enhanced, detection-friendly radar *hyper* point cloud  $\hat{P}_t$ . Our goal is to improve radar input quality by increasing measurement density and suppressing clutter/spurious reflections, while preserving radar-specific physical cues (e.g., Doppler velocity and Radar Cross-Section) and producing more structured, regular foreground geometry that is consistent with LiDAR-derived object structure under known calibration for downstream radar-only 3D object detection. Let  $\mathcal{R}_t = \{R_\tau^i \mid i = 1, \dots, N, \tau = t-k, \dots, t\}$  denote the set of radar sweeps collected from  $N$  surrounding radars over a temporal window of length  $k+1$ . Each sweep  $R_\tau^i$  is represented as a set of radar points  $\mathbf{p} = [x, y, z, r, v_d]$ , where  $(x, y, z)$  are 3D Cartesian coordinates,  $r$  is the radar cross-section (RCS), and  $v_d$  is the Doppler (radial) velocity. Accordingly, HyperDet takes  $\mathcal{R}_t$  as input and outputs the enhanced radar point cloud  $\hat{P}_t$ .

#### B. Overview

HyperDet is a compact three-stage radar-only 3D detection pipeline. As illustrated in Fig. 2, HyperDet takes raw multi-radar measurements within a short temporal window as input and outputs final 3D detections. The first stage performs spatio-temporal multi-radar fusion to improve input quality and construct a denoised point cloud, the second stage further enhances object-centric geometry via a LiDAR-guided diffusion model, and the third stage applies a LiDAR-compatible detector to produce 3D bounding boxes.

Specifically, HyperDet first aggregates consecutive sweeps from multiple surround-view radars in a unified reference frame to increase point density and spatial coverage, and jointly applies cross-sensor consensus validation to suppress clutter and spurious reflections, resulting in a denoised radar point cloud. Next, to further strengthen foreground structure, a conditional diffusion model operates on BEV radar features and enhances object regions under training-time LiDAR guidance while preserving radar-specific cues. Finally, the enhanced hyper point cloud is fed into standard 3D detectors (e.g., VoxelNeXt [15]) without modifying their architectures,

enabling HyperDet to leverage mature detection backbones and improve radar-only detection performance.

#### C. Spatio-Temporal Fusion and Cross-Sensor Validation

The goal of this stage is to address the key input bottlenecks of radar point clouds: extreme sparsity and multipath-induced noise. By constructing a unified and denoised spatio-temporal radar representation, we provide a stable foundation for subsequent enhancement and 3D detection. Formally, given the short-window multi-radar input  $\mathcal{R}_t$  defined in Sec. III-A, we produce a unified and denoised radar point cloud  $\tilde{R}_t = \mathcal{G}(\mathcal{R}_t; \Phi)$ , where  $\mathcal{G}$  denotes the fusion-and-validation module and  $\Phi$  collects calibration parameters, odometry information and filtering hyperparameters.

**Spatial Alignment.** To enable spatial fusion of multiple surround-view 4D radars, we transform all radar points into a unified reference frame using the provided extrinsic calibration. For radar  $i$ , let  $\mathbf{T}_{i \rightarrow \text{ref}}(t)$  denote the radar-to-reference transformation at time  $t$ . Given a radar point in homogeneous coordinates  $\tilde{\mathbf{p}} = [x, y, z, 1]^\top$ , its reference-frame coordinate is obtained by  $\tilde{\mathbf{p}}_{\text{ref}} = \mathbf{T}_{i \rightarrow \text{ref}}(t) \tilde{\mathbf{p}}$ . This step expresses multi-radar measurements in a common coordinate system, enabling geometrically consistent fusion and subsequent processing.

**Temporal Accumulation.** To mitigate the sparsity of single-sweep radar measurements, we aggregate consecutive sweeps within a short temporal window while compensating for ego-motion using the provided odometry. Specifically, for each radar  $i$ , we transform a past sweep at time  $\tau \in \{t-k, \dots, t\}$  to the keyframe  $t$  as

$$R_\tau^{i \rightarrow t} = \{\mathbf{T}_{\text{ref}}(t) \mathbf{T}_{\text{ref}}(\tau)^{-1} \tilde{\mathbf{p}} \mid \mathbf{p} \in R_\tau^i\}, \quad (1)$$

where  $\mathbf{T}_{\text{ref}}(t)$  denotes the ego pose (odometry) in the reference frame at time  $t$ . We then form the spatio-temporally accumulated 4D radar point cloud by

$$R_t^{\text{acc}} = \bigcup_{i=1}^N \bigcup_{\tau=t-k}^t R_\tau^{i \rightarrow t} \quad (2)$$

This ego-motion compensated accumulation increases point density and coverage, yielding a stronger input.

**Cross-Sensor Validation.** Spatio-temporal fusion substantially increases point density, but it also inevitably accumulates and amplifies sensor-specific noise across views and sweeps, including multipath-induced ghosts and isolated clutter. To mitigate this effect, we exploit the surround-view multi-radar setup and perform cross-sensor validation in regions with overlapping fields of view. The key intuition is that physically consistent returns are more likely to be corroborated by multiple radars, whereas spurious reflections often appear only in a single view. The detailed procedure is summarized in Algorithm 1. We validate each point using two complementary criteria. *Cross-sensor support* retains a point if there exists a nearby observation from any other radar within a distance threshold, which accounts for measurement noise and calibration uncertainty. However, not all true returns are multi-view observable due to occlusion

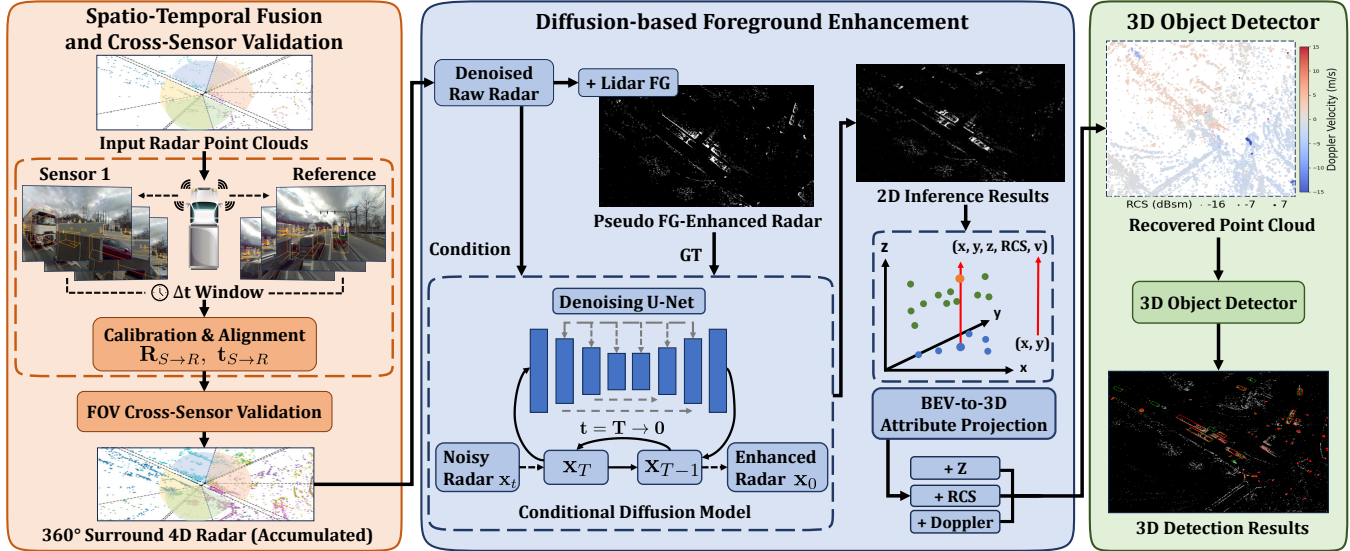


Fig. 2. Overview of the proposed HyperDet pipeline. Raw multi-radar measurements are (i) temporally and spatially aggregated and validated via cross-sensor consensus, (ii) enhanced through diffusion-based foreground refinement, and (iii) processed by a LiDAR-compatible 3D detector.

### Algorithm 1 Cross-Sensor Validation for Denoising

**Require:** Spatio-temporally accumulated point clouds  $\{R_t^{i,acc}\}_{i=1}^N$ , cross-sensor distance threshold  $\tau_d$ , neighborhood radius  $r$ , minimum neighbor count  $k$   
**Ensure:** Validated (denoised) radar point cloud  $\tilde{R}_t$

- 1:  $\tilde{R}_t \leftarrow \emptyset$
- 2: **for**  $i = 1$  **to**  $N$  **do**
- 3:   **for** each point  $\mathbf{p}_a \in R_t^{i,acc}$  **do**
- 4:      $\text{cross} \leftarrow \exists j \in \{1, \dots, N\} \setminus \{i\}, \exists \mathbf{p}_b \in R_t^{j,acc} : \|\mathbf{p}_a - \mathbf{p}_b\|_2 < \tau_d$
- 5:      $\text{self} \leftarrow (|\mathcal{N}_r(\mathbf{p}_a; R_t^{i,acc})| \geq k)$
- 6:     **if**  $\text{cross}$  **or**  $\text{self}$  **then**
- 7:        $\tilde{R}_t \leftarrow \tilde{R}_t \cup \{\mathbf{p}_a\}$
- 8:     **end if**
- 9:   **end for**
- 10: **end for**
- 11: **return**  $\tilde{R}_t$

and view-dependent scattering; thus, we additionally apply a *self-consistency* criterion that preserves points forming a sufficiently dense local cluster. Together, these rules suppress clutter and ghost reflections while avoiding over-filtering sparse yet valid measurements, producing a cleaner point cloud for subsequent diffusion-based enhancement and downstream 3D detection.

### D. Diffusion-based Foreground Enhancement

Spatio-temporal fusion and cross-sensor validation improve radar input quality by increasing density and suppressing multi-path clutter. However, the resulting point cloud  $\tilde{R}_t$  is still sparse and irregular, and a non-negligible portion of noisy returns remains unverifiable, especially outside overlapping views. Consequently, foreground geometry is weak and unstable, continuing to limit accurate 3D box regression. This issue is amplified by the extreme foreground sparsity of radar: on MAN TruckScenes [14], fewer than 2% of radar points fall inside annotated 3D boxes, compared to around

10% for LiDAR sweeps.

To mitigate the sparsity issues, prior work often performs global radar super-resolution to produce LiDAR-like dense reconstructions [12], [43], but optimizing global density is typically background-dominated, increases model burden, and may introduce details that are less relevant (or harmful) to detection. In contrast, we perform *object-centric foreground enhancement*: we selectively densify and regularize foreground shapes that matter for box regression, while keeping the radar background largely unchanged and preserving radar-specific cues. Concretely, we adopt an EDM-based conditional diffusion model [45] in BEV space to enhance the radar foreground part with LiDAR supervision.

**LiDAR-Guided Enhancement.** We use LiDAR *only during training* to construct dense foreground supervision for diffusion learning. We remove LiDAR ground points [46] and extract foreground points inside annotated 3D bounding boxes. To make the supervision radar-aware, for each box we compute the mean RCS and Doppler values from  $\tilde{R}_t$  (validated radar returns) within the same region and assign them to the LiDAR foreground points, forming a *pseudo-radar* foreground  $\tilde{F}_t$ . We then build the diffusion target point cloud by injecting  $\tilde{F}_t$  into  $\tilde{R}_t$  while keeping the radar background unchanged, so the model focuses on object-level enhancement rather than global reconstruction.

**Diffusion Model Training.** To leverage the strong inductive bias and computational efficiency of image diffusion models, we perform generative enhancement in the BEV space, where the radar point cloud is rasterized into a 2D grid representation. We adopt the Elucidated Diffusion Model (EDM) [45] as our conditional generative backbone in BEV space. Let  $\mathbf{c} = \text{BEV}(\tilde{R}_t)$  be the BEV condition extracted from the validated radar input, and let  $\mathbf{x}_0 = \text{BEV}(\tilde{R}_t \oplus \tilde{F}_t)$  denote the LiDAR-guided target BEV after foreground injection.<sup>1</sup> EDM perturbs  $\mathbf{x}_0$  with Gaussian noise at a sampled noise

<sup>1</sup>  $\oplus$  denotes foreground injection that preserves the radar background.

level  $\sigma(t)$ :

$$\mathbf{x}_t = \mathbf{x}_0 + \sigma(t) \epsilon, \quad \epsilon \sim \mathcal{N}(0, \mathbf{I}), \quad (3)$$

and trains a noise-conditioned network to recover  $\mathbf{x}_0$  from  $(\mathbf{x}_t, t, \mathbf{c})$  using a conditional MSE loss:

$$\mathcal{L}_{\text{diff}} = \mathbb{E}_{t, \epsilon} \left[ \left\| \mathbf{x}_0 - \mathbf{x}_\theta(\mathbf{x}_t, t, \mathbf{c}) \right\|_2^2 \right]. \quad (4)$$

The denoiser  $\mathbf{x}_\theta$  is parameterized by a U-Net [38] (with residual blocks and attention following [12]) conditioned on the diffusion timestep.

**Inference and Point Cloud Recovery.** At inference, the model takes radar-only inputs and outputs an enhanced BEV foreground map conditioned on  $\mathbf{c}$ . We threshold the predicted BEV to obtain 2D foreground point coordinates  $(x, y)$ ; the predicted intensity is treated as a confidence score. To obtain a full 4D radar point cloud, we lift each generated  $(x, y)$  by inheriting  $(z, \text{RCS}, v_d)$  from its nearest neighbor in the validated radar point cloud. This attribute lifting preserves radar-specific physical cues while benefiting from the enhanced foreground geometry.

**Efficiency via Consistency Distillation.** Iterative diffusion sampling can be computationally expensive. We therefore distill the trained diffusion model into a consistency model [13] with the same architecture, enabling efficient single-step generation at inference while maintaining diffusion-quality enhancement.

### E. 3D Object Detector

Our point cloud enhancement method is detector-agnostic and can be applied to any LiDAR-based 3D detectors. In practice, we feed the enhanced radar hyper point cloud into standard LiDAR-based 3D object detectors (e.g., CenterPoint [16] and VoxelNeXt [15]) without architectural modification. Please see IV-A for more implementation details.

## IV. EXPERIMENT

### A. Experimental Setup

**Dataset.** All experiments are conducted on the MAN TruckScenes dataset [14], which provides six synchronized 4D mmWave radars (20 Hz) mounted at different locations on a heavy-duty truck, enabling full 360° coverage. We use the official split (70%/10%/20% for train/val/test), resulting in  $\sim 30k$  radar–LiDAR sample pairs from 747 scenes. We use three out of six LiDARs from MAN TruckScenes which are co-located with the radars and jointly cover the full surround view. A single LiDAR sweep is sufficiently dense and used to extract the supervision.

**Evaluation Protocol.** (1) *Diffusion enhancement.* We evaluate geometric reconstruction quality against the LiDAR-guided foreground target in BEV using Chamfer Distance (CD), Hausdorff Distance (HD), and F-score under a fixed matching threshold. (2) *3D detection.* We follow the official MAN TruckScenes protocol and report mAP and NDS [3] on seven primary categories: *car*, *truck*, *other vehicle*, *trailer*, *traffic sign*, *traffic cone*, and *pedestrian*. mAP averages AP over center-distance thresholds  $\mathcal{D} = \{0.5, 1, 2, 4\}$  meters. To

TABLE I  
FOREGROUND POINTS ENHANCEMENT INSIDE 3D BOXES  
(AVG./SAMPLE) ON MAN TRUCKSCENES.

Class	Raw	Avg	Added Avg ( $\Delta$ )	Boost ( $\Delta/\text{Raw}$ ) $\uparrow$
Car	6.13	+11.71		185.47%
Truck	31.31	+27.50		87.83%
Other vehicle	98.70	+63.24		64.08%
Trailer	78.72	+95.60		121.45%
Traffic sign	4.50	+1.26		27.93%
Traffic cone	0.92	+0.27		29.44%
Pedestrian	4.85	+1.70		35.11%
<b>Total FG ratio increase</b>	<b>575.81</b>	<b>662.40</b>		<b>115.04%</b>

TABLE II  
ABLATION OF DIFFUSION SUPERVISION. LOWER CD/HD AND HIGHER  
F-SCORE INDICATE BETTER GEOMETRIC FIDELITY. THE NUMBERS  
(128/512) DENOTE THE BEV RESOLUTION USED DURING SUPERVISION,  
WHERE HIGHER RESOLUTION PROVIDES FINER SPATIAL TARGETS.

Supervision Target	CD $\downarrow$	HD $\downarrow$	F-score $\uparrow$
LiDAR FG only (512)	8.3224	32.7222	0.3399
LiDAR FG + radar (128)	2.0412	16.0697	0.7612
LiDAR FG + radar CD (512)	0.1689	7.6858	0.8140
LiDAR FG + radar (512)	0.0974	4.4692	0.9047

match the diffusion BEV range and radar sensing characteristics, all detection evaluations are performed within 50 m maximum range.

**Implementation Details.** Radar point clouds are temporally accumulated over a 0.5 s window (equally 10 frames), and all points are transformed into the unified `LIDAR_LEFT` frame. For the cross-sensor validation (c.f. Sec. 1),  $\tau_d$  is set as 10 m,  $r$  is 1 m while  $k$  is 3. Due to severe self-occlusion from the truck body, we reduce the effective FoV of the two rear radars from 120° to 100° to avoid over-filtering valid returns in partially occluded regions. For diffusion, both the validated radar representation and the LiDAR-guided target are rasterized into 512 × 512 BEV images covering [−50, 50] m in both  $x$  and  $y$ , corresponding to 0.195 m per pixel. Each pixel encodes binary occupancy (0 for empty, 255 for occupied). At inference, we threshold the predicted BEV at an intensity of 60 to extract confident foreground regions. For 3D detection, We use VoxelNeXt [15] and CenterPoint [16] implemented in OpenPCDet [47]. Unless otherwise stated, detectors are trained for 20 epochs on the official split with identical optimization schedules and data augmentations across all inputs, so differences are attributable to input quality.

### B. Quantitative Results

Our goal is to improve radar input representations without modifying LiDAR-oriented detector. We therefore first evaluate whether the proposed diffusion module can increase foreground density and improve foreground geometry, and then examine how these improvements translate to downstream 4D radar-only 3D detection. Unless otherwise stated, all comparisons keep the 3D detector unchanged and only vary the radar inputs.

**Diffusion-Based Foreground Enhancement.** We begin by

validating that the diffusion-based foreground enhancement module (c.f. Sec. III-D) indeed strengthens object-centric foreground structure. As discussed in Sec. III-D, the model is trained with a foreground-injected supervision target (LiDAR-derived foreground + validated radar background), and uses radar-only inputs at inference. We first measure the change of *foreground point density* by counting radar points falling inside annotated 3D boxes. Table I reports the average number of foreground points per frame for each class. Our approach consistently increases effective radar foreground occupancy across categories, with particularly large gains on structurally salient objects (e.g., *car/truck/trailer*), indicating that diffusion recovers missing foreground support beyond deterministic fusion and filtering. Increasing point counts alone can be misleading; we therefore further evaluate *geometric fidelity* against the LiDAR-guided foreground reference. As shown in Table II, HyperDet achieves low CD/HD and a high F-score, suggesting that the added foreground structure is coherent and well-aligned rather than spurious. We also note that using a higher-resolution BEV supervision leads to consistently lower CD and HD, as finer spatial discretization enables more accurate foreground geometry reconstruction. Together, these results confirm that our diffusion module improves radar foreground *both in density and quality*, providing a stronger input for 3D box regression.

**Radar-Only 3D Detection Performance.** We next evaluate whether the enhanced radar representation improves downstream radar-only 3D detection. Table III reports results with two LiDAR-oriented detectors (VoxelNeXt [15] and CenterPoint [16]) *without any architectural modification*, so the performance differences are attributable to the input representation. As a minimal reference, we use the raw single-sweep radar point cloud as the baseline input.

HyperDet significantly improves radar-only performance across both detectors, demonstrating that its temporal fusion, cross-sensor validation, and object-centric diffusion enhancement yield detection-relevant gains beyond raw radar data. With VoxelNeXt, HyperDet raises mAP from 0.0619 to 0.1311, confirming that enhanced foreground completeness and regularity directly improve 3D box regression. For reference, we also include single-sweep LiDAR results and an oracle mixture of radar background with LiDAR foreground. While not radar-only, these establish performance upper bounds and further highlight foreground quality as a key bottleneck in radar detection. Consistent improvements across VoxelNeXt and CenterPoint indicate the gains originate from better inputs rather than detector-specific biases, framing HyperDet as a detector-agnostic radar perception front-end.

### C. Ablation Studies

We ablate the key design choices in HyperDet: (i) temporal accumulation, (ii) cross-sensor validation, (iii) diffusion-based foreground enhancement, and (iv) BEV-to-point reconstruction. Unless otherwise specified, all ablations are evaluated on the MAN TruckScenes test split using a fixed detector backbone (VoxelNeXt) so that performance

TABLE III  
3D OBJECT DETECTION PERFORMANCE. BASELINE INDICATES THE INPUT TO BE RAW SINGLE-SWEEP 4D RADAR POINT CLOUD. MIXED INDICATES RADAR BG + LiDAR FG.

Input	3D Detector	mAP	NDS
Baseline	VoxelNeXt	0.0619	0.1663
HyperDet w.o. Diffusion	VoxelNeXt	0.1240	0.2188
HyperDet	VoxelNeXt	0.1311	0.2217
Baseline	CenterPoint	0.0688	0.1724
HyperDet w.o. Diffusion	CenterPoint	0.1221	0.2149
HyperDet	CenterPoint	0.1225	0.2210
1-sweep LiDAR	VoxelNeXt	0.2419	0.2755
Mixed R&L	VoxelNeXt	0.2637	0.3036

TABLE IV  
EFFECT OF ACCUMULATION AND CROSS-SENSOR VALIDATION.

Temp. Accum.	CS. Val.	mAP	NDS
		0.0619	0.1663
	✓	0.0613	0.1646
✓		0.1230	0.2174
✓	✓	0.1240	0.2188

differences reflect changes in the radar input representation rather than detector design.

**Temporal Accumulation and Cross-Sensor Validation.** Table IV isolates the impact of temporal accumulation and cross-sensor validation. With a single sweep, radar returns are extremely sparse, and validation may discard isolated yet correct measurements, leading to a slight drop in mAP/NDS. Temporal accumulation substantially improves point density and foreground coverage, which largely accounts for the performance jump. Given accumulated inputs, cross-sensor validation becomes consistently beneficial: it suppresses multipath-induced clutter amplified by spatio-temporal fusion and stabilizes object-centric geometry, yielding additional gains on top of temporal fusion.

**Diffusion Supervision Design.** In Table II, We compare two training targets for diffusion: using LiDAR foreground only versus our *foreground-injection* target that preserves the validated radar background while injecting LiDAR-derived foreground geometry. LiDAR-only targets provide clean shapes but discard radar-specific background occupancy and clutter statistics, which can make the learned prior less consistent with radar-only inputs at inference. In contrast, foreground injection retains radar background structure and explicitly localizes where enhancement is required, encouraging the model to focus capacity on object geometry while remaining compatible with radar-only observations.

**BEV-to-Point Cloud Recovery.** After diffusion, we convert the predicted  $512 \times 512$  BEV occupancy into a 3D radar *hyper* point cloud for detection. Table V shows that naively increasing point density via heuristic filling can *hurt* detection. While filling increases the number of points, it can also over-amplify uncertain regions and introduce geometrically plausible-but-unsupported structures, which dominate the detector input and degrade localization, especially around cluttered backgrounds and small objects. A higher threshold reduces such over-generation but may under-recover weak foreground. Overall, the best trade-off is achieved

TABLE V

EFFECTS OF BEV-TO-POINT RECOVERY DENSITY ON DETECTION PERFORMANCE. HIGHER MAP / NDS INDICATE BETTER QUALITY.

Reconstruction Setting	mAP	NDS
Threshold = 60, no point filling	0.1311	0.2217
Threshold = 60, with point filling	0.1274	0.2113
Threshold = 200, with point filling	0.1253	0.2097

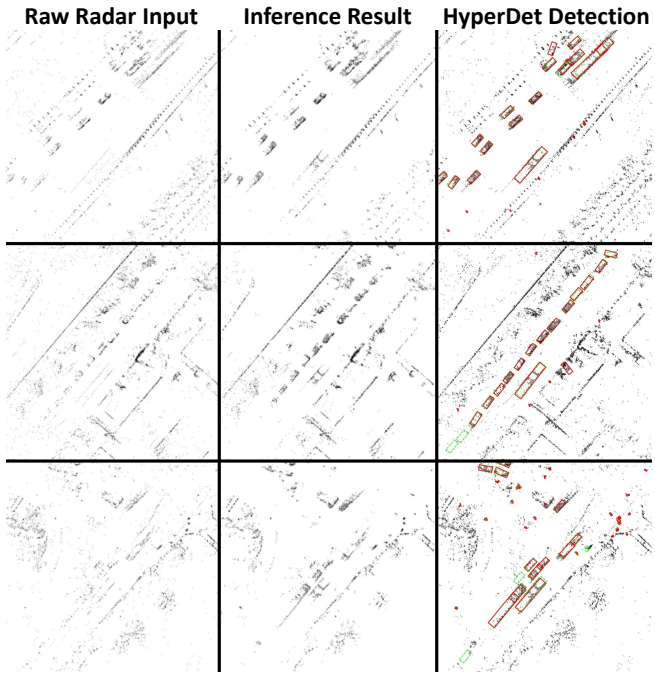


Fig. 3. Qualitative results of radar enhancement: raw radar input vs. diffusion-enhanced output vs. HyperDet detection results. Red boxes denote predictions; green boxes denote ground truth.

by thresholding without aggressive point filling, indicating that reconstruction should preserve radar-consistent sparsity and rely on diffusion (rather than heuristics) to add reliable foreground structure.

#### D. Qualitative Results

We provide qualitative visualizations of (i) diffusion-based radar enhancement and (ii) downstream radar-only 3D object detection to illustrate the effect of HyperDet in practice.

**Qualitative Analysis.** Fig. 3 qualitatively compares the validated spatio-temporal fused radar input, the HyperDet-enhanced radar *hyper* point cloud, and the resulting radar-only 3D detections. For near-range targets, HyperDet increases foreground density and regularizes object geometry, yielding more coherent shapes that better align with LiDAR supervision and support more stable 3D box regression. The enhanced hyper point clouds produce more robust detections for nearby vehicles, especially moving objects benefiting from temporal consistency. Distant targets remain challenging due to sparse radar evidence and may suffer from orientation errors, but confidence and localization generally improve over raw radar. For small objects (e.g., pedestrians), HyperDet can sometimes recover sufficient structure to enable detection, although false positives and unstable orientations persist.

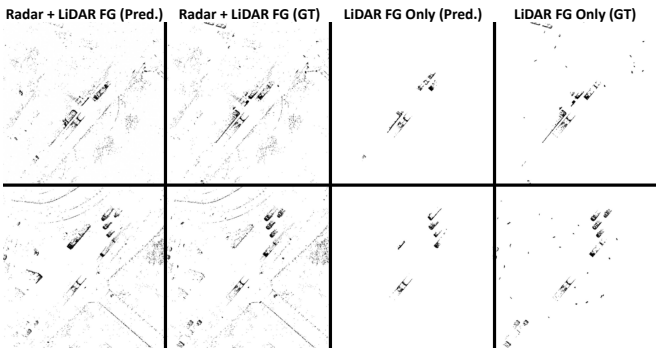


Fig. 4. Comparison of diffusion enhancement under different supervision.

**Effect of Diffusion Supervision.** Fig. 4 highlights how supervision design affects diffusion behavior. When trained with LiDAR-foreground supervision alone, the model tends to produce surface-like, shell structures and exhibits less stable localization, reflecting the inherent surface-biased distribution of LiDAR returns and the lack of radar-specific anchoring cues. Moreover, motion-induced streaking from temporal fusion can bias the enhancement direction, leading to spatial offsets in challenging cases. In contrast, the merged target (*LiDAR-FG + raw radar background*) provides complementary constraints: radar observations act as geometric anchors and background priors, while LiDAR foreground supplies dense object-level structure. This combination yields more coherent and spatially consistent foreground shapes and reduces ambiguity under sparse radar returns.

**Failure Modes.** Diffusion-based enhancement cannot recover objects that are largely missing in the radar input; it refines and densifies *observed* structures rather than hallucinating unseen targets. In addition, strong reflections from static background structures may resemble vehicle-like patterns; in these cases, enhancement can amplify spurious clusters and create hard negatives for the detector.

#### E. Runtime Efficiency

Table VI reports the component-wise computation cost of HyperDet. Spatio-temporal fusion and cross-sensor validation are lightweight, with negligible FLOPs and memory usage and a combined latency under 40 ms. The diffusion module constitutes the main computational bottleneck: the teacher model requires a 40-step denoising process, resulting in extremely high cost and latency. Our consistency-distilled student compresses the 40-step teacher into a single-step model, reducing diffusion latency by more than 70-fold while preserving accuracy. The VoxelNeXt detector adds only 43 ms. Overall, the distilled pipeline achieves a 151 ms end-to-end latency, making near real-time deployment feasible.

## V. CONCLUSION

We presented HyperDet, a detector-agnostic radar-only 3D detection pipeline that improves radar perception at the *input level*. HyperDet constructs a task-aware *hyper* 4D radar point cloud via hierarchical input refinement pipeline. Experiments on MAN TruckScenes with different types of LiDAR-oriented detectors show consistent gains over raw

TABLE VI

COMPONENT-WISE COMPUTATION COST OF HYPERDET. LATENCY  
MEASURED ON AN RTX 4090.

Component	GFLOPs	Mem (MB)	Latency (ms)
Spatio-temporal fusion	$\sim 0$	0.001	6.07
Cross-sensor validation	$\sim 0$	0.001	32.74
Diffusion (teacher)	$2.49 \times 10^4$	436.40	5008.78
Diffusion (CD student)	$3.15 \times 10^2$	428.40	68.97
VoxelNeXt detector	5.05	123.76	43.24
<b>Total (teacher)</b>	$2.49 \times 10^4$	560.16	5090.83
<b>Total (CD)</b>	$3.20 \times 10^2$	552.16	151.02

radar inputs without modifying the detectors, partially narrowing the radar–LiDAR performance gap.

**Limitations and Future Work.** Performance remains limited by moderate training data size, sparse evidence for distant or small objects and severe multipath noises, and diffusion cannot recover targets that are largely missing in the radar input. In addition, the current BEV-based diffusion discards vertical information and assumes a single height per BEV location, limiting multi-layer scene representation (e.g., vehicles under overpasses). Future work will improve attribute modelling, robustness and generalization across radar setups, and explore 3D diffusion with tighter temporal and Doppler integration for richer scene understanding.

## REFERENCES

- [1] J. Mao, S. Shi, X. Wang, and H. Li. 3d object detection for autonomous driving: A comprehensive survey. *IJCV*, 2023.
- [2] J. Karangwa, J. Liu, and Z. Zeng. Vehicle detection for autonomous driving: A review of algorithms and datasets. *T-ITS*, 2023.
- [3] H. Caesar, V. Bankiti, A. H. Lang, S. Vora, V. E. Liang, Q. Xu, A. Krishnan, Y. Pan, G. Baldan, and O. Beijbom. nuscenes: A multimodal dataset for autonomous driving. In *CVPR*, 2020.
- [4] A. Palffy, E. Pool, S. Baratam, J. F. P. Kooij, and D. M. Gavrila. Multi-class road user detection with 3+1d radar in the view-of-delft dataset. *RA-L*, 2022.
- [5] M. Jiang, G. Xu, H. Pei, Z. Feng, S. Ma, H. Zhang, and W. Hong. 4d high-resolution imagery of point clouds for automotive mmwave radar. *T-ITS*, 2024.
- [6] L. Fan, J. Wang, Y. Chang, Y. Li, Y. Wang, and D. Cao. 4d mmwave radar for autonomous driving perception: A comprehensive survey. *T-IV*, 2024.
- [7] Y. Zhou, J. Hao, and K. Zhu. Rmsa-net: A 4d radar based multi-scale attention network for 3d object detection. In *ISCSIC*, 2023.
- [8] A. Musiat, L. Reichardt, M. Schulze, and O. Wasenmüller. Radarpillars: Efficient object detection from 4d radar point clouds. In *ITSC*, 2024.
- [9] J. Li, L. Yang, Y. Chen, Y. Yang, Y. Jin, and K. Akiyama. Pillardan: Pillar-based dual attention attention network for 3d object detection with 4d radar. In *ITSC*, 2023.
- [10] A. Venon, Y. Dupuis, P. Vasseur, and P. Merriaux. Millimeter wave fmew radars for perception, recognition and localization in automotive applications: A survey. *T-IV*, 2022.
- [11] Y. Song, J. Sohl-Dickstein, D. P. Kingma, A. Kumar, S. Ermon, and B. Poole. Score-based generative modeling through stochastic differential equations. *arXiv*, 2020.
- [12] R. Zhang, D. Xue, Y. Wang, R. Geng, and F. Gao. Towards dense and accurate radar perception via efficient cross-modal diffusion model. *RA-L*, 2024.
- [13] Y. Song, P. Dhariwal, M. Chen, and I. Sutskever. Consistency models. 2023.
- [14] F. Fent, F. Kuttnerreich, F. Ruch, F. Rizwin, S. Juergens, L. Lechermann, C. Nissler, A. Perl, U. Voll, and M. et al. Yan. Man truckscenes: A multimodal dataset for autonomous trucking in diverse conditions. *NeurIPS*, 2024.
- [15] Y. Chen, J. Liu, X. Zhang, X. Qi, and J. Jia. Voxelnext: Fully sparse voxelnet for 3d object detection and tracking. In *CVPR*, 2023.
- [16] T. Yin, X. Zhou, and P. Krahenbuhl. Center-based 3d object detection and tracking. In *CVPR*, 2021.
- [17] A. Ghasemieh and R. Kashef. 3d object detection for autonomous driving: Methods, models, sensors, data, and challenges. *TE*, 2022.
- [18] G. Zamanakos, L. Tsochatzidis, A. Amanatidis, and I. Pratikakis. A comprehensive survey of lidar-based 3d object detection methods with deep learning for autonomous driving. *Computers & Graphics*, 2021.
- [19] N. H. H. Aung, P. Sangwongngam, R. Jintamethasawat, S. Shah, and L. Wuttisittikulij. A review of lidar-based 3d object detection via deep learning approaches towards robust connected and autonomous vehicles. *IEEE T-IV*, 2024.
- [20] S. Y. Alaba and J. E. Ball. A survey on deep-learning-based lidar 3d object detection for autonomous driving. *Sensors*, 2022.
- [21] Y. Zhou and O. Tuzel. Voxelnet: End-to-end learning for point cloud based 3d object detection. In *CVPR*, 2018.
- [22] Y. Yan, Y. Mao, and B. Li. Second: Sparsely embedded convolutional detection. *Sensors*, 2018.
- [23] A. H. Lang, S. Vora, H. Caesar, L. Zhou, J. Yang, and O. Beijbom. Pointpillars: Fast encoders for object detection from point clouds. In *CVPR*, 2019.
- [24] Y. Wu, Y. Wang, S. Zhang, and H. Ogai. Deep 3d object detection networks using lidar data: A review. *SensorsJ*, 2021.
- [25] D.-H. Paek, S.-H. Kong, and K. T. Wijaya. K-radar: 4d radar object detection for autonomous driving in various weather conditions. *NeurIPS*, 2022.
- [26] L. Zheng, Z. Ma, X. Zhu, B. Tan, S. Li, K. Long, W. Sun, S. Chen, L. Zhang, and M. et al. Wan. Tj4dradset: A 4d radar dataset for autonomous driving. In *ITSC*, 2022.
- [27] N. Scheiner, F. Kraus, N. Appenrodt, J. Dickmann, and B. Sick. Object detection for automotive radar point clouds—a comparison. *AIP*, 2021.
- [28] B. Tan, Z. Ma, X. Zhu, S. Li, L. Zheng, S. Chen, L. Huang, and J. Bai. 3-d object detection for multiframe 4-d automotive millimeter-wave radar point cloud. *SensorsJ*, 2022.
- [29] P. Palmer, M. Krueger, R. Altendorfer, and T. Bertram. Ego-motion estimation and dynamic motion separation from 3d point clouds for accumulating data and improving 3d object detection. In *AmE*, 2023.
- [30] S.-H. Kong, D.-H. Paek, and S. Cho. Rtnh+: Enhanced 4d radar object detection network using combined cfar-based two-level preprocessing and vertical encoding. *arXiv*, 2023.
- [31] F. Fent, P. Bauerschmidt, and M. Lienkamp. Radargnn: Transformation invariant graph neural network for radar-based perception. In *CVPR*, 2023.
- [32] Mark A Richards et al. *Fundamentals of radar signal processing*, volume 1. McGraw-Hill New York, 2005.
- [33] D. Brodeski, I. Bilik, and R. Giryes. Deep radar detector. In *RadarConf*, 2019.
- [34] M. Chamseddine, J. Rambach, D. Stricker, and O. Wasenmüller. Ghost target detection in 3d radar data using point cloud based deep neural network. In *ICPR*, 2021.
- [35] C. R. Qi, H. Su, K. Mo, and L. J. Guibas. Pointnet: Deep learning on point sets for 3d classification and segmentation. In *CVPR*, 2017.
- [36] M. Mirza and S. Osindero. Conditional generative adversarial nets. *arXiv*, 2014.
- [37] J. Guan, S. Madani, S. Jog, S. Gupta, and H. Hassanieh. Through fog high-resolution imaging using millimeter wave radar. In *CVPR*, 2020.
- [38] O. Ronneberger, P. Fischer, and T. Brox. U-net: Convolutional networks for biomedical image segmentation. In *MICCAI*, 2015.
- [39] A. Prabhakara, T. Jin, A. Das, G. Bhatt, L. Kumari, E. Soltanaghaei, J. Bilmes, S. Kumar, and A. Rowe. High resolution point clouds from mmwave radar. *arXiv*, 2022.
- [40] Y. Cheng, J. Su, M. Jiang, and Y. Liu. A novel radar point cloud generation method for robot environment perception. *T-RO*, 2022.
- [41] R. Geng, Y. Li, D. Zhang, J. Wu, Y. Gao, Y. Hu, and Y. Chen. Dream-pcd: Deep reconstruction and enhancement of mmwave radar pointcloud. *TIP*, 2024.
- [42] C. X. Lu, S. Rosa, P. Zhao, B. Wang, C. Chen, J. A. Stankovic, N. Trigoni, and A. Markham. See through smoke: robust indoor mapping with low-cost mmwave radar. In *Proceedings of the 18th International Conference on Mobile Systems, Applications, and Services*, 2020.
- [43] K. Luan, C. Shi, N. Wang, Y. Cheng, H. Lu, and X. Chen. Diffusion-based point cloud super-resolution for mmwave radar data. In *ICRA*, 2024.

- [44] Y. Liu, X. Chen, N. Wang, S. Andreev, A. Dvorkovich, R. Fan, and H. Lu. Self-supervised diffusion-based scene flow estimation and motion segmentation with 4d radar. *RA-L*, 2025.
- [45] T. Karras, M. Aittala, T. Aila, and S. Laine. Elucidating the design space of diffusion-based generative models. *NeurIPS*, 2022.
- [46] S. Lee, H. Lim, and H. Myung. Patchwork++: Fast and robust ground segmentation solving partial under-segmentation using 3d point cloud. In *IROS*, 2022.
- [47] OpenPCDet Development Team. Openpcdet: An open-source toolbox for 3d object detection from point clouds. <https://github.com/open-mmlab/OpenPCDet>, 2020.